

Open-slip coupled model for simulating three-dimensional bond behavior of reinforcing bars in concrete

Feng Shang¹, Xuhui An*¹, Seji Kawai¹ and Tetsuya Mishima²

¹State Key Laboratory of Hydro Science and Engineering, Tsinghua University,
100084-Beijing, China

²Maeda Corporation, Tokyo, Japan

(Received June 15, 2009, Accepted March 23, 2010)

Abstract. The bond mechanism for reinforcing bars in concrete is equivalent to the normal contact and friction between the inclined ribs and the surrounding concrete. Based on the contact density model for the computation of shear transfer across cracks, an open-slip coupled model was developed for simulating three-dimensional bond behavior for reinforcing bars in concrete. A parameter study was performed and verified by simulating pull-out experiments of extremely different boundary conditions: short bar embedment with a huge concrete cover, extremely long bar embedment with a huge concrete cover, embedded aluminum bar and short bar embedded length with an insufficient concrete cover. The bar strain effect and splitting of the concrete cover on a local bond can be explained by finite element (FE) analysis. The analysis shows that the strain effect results from a large local slip and the splitting effect of a large opening of the interface. Finally, the sensitivity of rebar geometry was also checked by FE analysis and implies that the open-slip coupled model can be extended to the case of plain bar.

Keywords: bond; open-slip coupled model; strain effect; splitting effect; bar geometry.

1. Introduction

For many decades, enormous experimental efforts have been made to study the bond of reinforcing bars in concrete (Goto 1971, Tassios and Yannopoulos 1981, Hawkins *et al.* 1982, Chou *et al.* 1983, Shima *et al.* 1987, Gambarova *et al.* 1989, Xu *et al.* 1994). Among these researchers, Chou *et al.* (1983) were the first to discuss the effect of reinforcing bar strain on local bond stress transfer that illustrates the effects of embedded length, location on a bar and its stiffness, and Shima *et al.* (1987) further proposed the unique bond-slip-strain model which covers both elastic and post-yielding ranges of rebar. Local bar strain was recognized as an indicator of the damage level of the surrounding concrete, which could be equivalent to the average strain of concrete including several Goto cracks (Maekawa *et al.* 2003). The authors fully accepted this concept (denoted as the strain effect in the context below) and adopted it for the bond modeling in this paper.

However, the effect of splitting cracks was intentionally avoided in Shima *et al.*'s experiments using a large concrete cover (diameter up to 0.5 m). It is well known that local bond performance can deteriorate significantly due to splitting cracks along the reinforcing bar. Thus, the coupling effect of the splitting cracks and the rebar strain, i.e. Goto cracks (Fig. 1) have to be determined.

* Corresponding author, Professor, E-mail: anxue@tsinghua.edu.cn

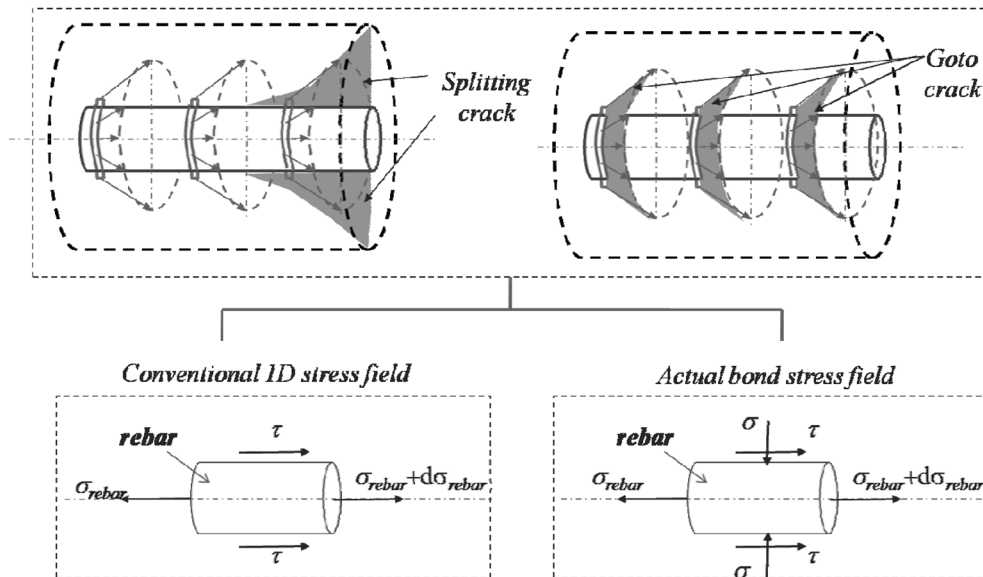


Fig. 1 Coupling effect of Goto cracks and splitting cracks

The effect of bond deterioration due to the splitting of the concrete cover is denoted as the splitting effect in the context below.

Gambarova *et al.* (1989) used a short pull-out experiment with an artificial splitting crack and related the bond-slip function to splitting crack width and macro-confining pressure between the reinforcing bar and the concrete. In this model, the inducement of a splitting crack due to the bond mechanism was not included. Xu *et al.* (1994) conducted hundreds of pull-out experiments and studied the bond strength at four critical stages: initial sliding of the free end, splitting of the cover, peak stage and residual stage. The design code for anchorage in concrete was established in China based on his results. It was found here that the bond strength just before the splitting of the concrete cover was proportional to $(C/d)^{1/2}$. C means the size of the concrete cover and d means the diameter of the reinforcing bar.

Both of these findings were based on a short bar embedded test, i.e. the strain effect is not included. As a unique constitutive law, the bond model should be independent with such boundary conditions as embedment length, locations along the reinforcing bar, splitting crack width and C/d . Thus, a universal bond model is still required.

Numerical works can also be helpful in studying bond mechanism (Teng *et al.* 1996, Cox *et al.* 1998, Ayoub and Filippou 1999, Lura *et al.* 2002, Salem *et al.* 2003, Jendele and Cervenka 2006, Ragueneau *et al.* 2006). The bar-concrete interface appears here as a one-dimensional stress-strain field (Fig. 1) when the reinforcing bar is modeled as a truss element, which could only be used with the application of a conventional bond-slip relationship (Jendele and Cervenka 2006). Therefore, the reinforcing bar should be modeled as a quadrilateral solid element, with not only local slip but local radial deformation of the interface incorporated in the computation. Most of the previous attempts were based on 2D FE analysis, which has difficulty describing the splitting effects of the concrete cover. Lura *et al.* (2002) developed a 3D bond model to simulate the propagation of splitting cracks in the concrete cover based on the assumption of a kinematic relation for the nodes of the interface

element. However, such an empirical formulation and parameters could hardly be extended to different cases.

Therefore, the main purpose of this paper is to develop a bond model for 3D FE analysis that can describe both strain and splitting effects. As discussed, to describe the splitting effect, bond stress (tangent to the interface) and the radial confinement stress around the rebar (normal to the interface) have to be taken into account. In the context of this paper, the tangent displacement at the interface is as the “local slip”, and the normal displacement at the interface is termed “local opening”.

2. Open-slip coupled modeling of bond

2.1 Modeling of normal contact between inclined rib and concrete

The physical mechanism of bond stress transfer is equivalent to an open-slip of the interface between the reinforcing bar and concrete. (Fig. 2) For 3D FE analysis, the shape of the bar is idealized as a cylinder, with the modeling of the interaction between the inclined rib and the concrete substituted for in the interface element, which has no volume. It was found that the open-slip of the interface induces normal contact and local friction between the inclined rib and surrounding concrete. Notably, the physical image of the bond is quite similar to that of the cracking shear transfer, which is controlled by the open-slip of cracking surface. Thus, the bond model can benefit greatly from the contact density model (Li and Maekawa 1989) for cracking shear transfer problems.

The relative displacement in both normal and tangential directions along the inclined rib (compression side) can be computed from the local opening and local slip of the interface as follows

$$\begin{cases} u_n = \delta \sin \theta - \omega \cos \theta \\ v_n = \delta \cos \theta + \omega \sin \theta \end{cases} \quad (1)$$

where ω and δ are the local opening and local slip of the interface, while u_n and v_n are the relative normal and tangential displacements, respectively; θ is the inclined angle of the rib.

Despite very accurate constitutive laws of such normal contact and local friction can hardly be obtained directly from an experiment, it is still possible to have a reasonable and simple assumption. The normal contact stress σ_n^0 at the free end with zero bar strain is assumed to be related only to the relative normal displacement u_n and governed by an elasto-plastic model (Fig. 3), which is expressed as follows

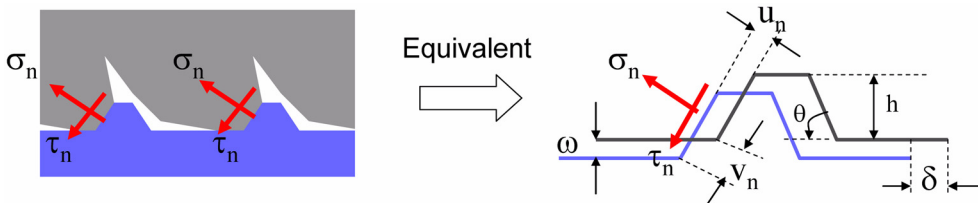


Fig. 2 Equivalent open-slip of interface between reinforcing bar and concrete

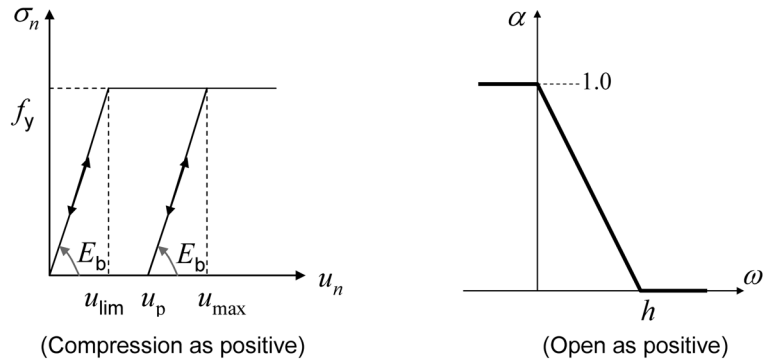


Fig. 3 Constitutive laws for normal contact between rib and concrete at location with zero strain

$$\sigma_n^0 = f(u_n) = \begin{cases} \alpha E_b(u_n - u_p), & u_n \geq u_p \\ 0, & u_n < u_p \end{cases} \quad (2)$$

where E_b means the stiffness of normal contact; α means the effective contact area between the inclined rib and the surrounding concrete, which is computed according to geometric relation (Fig. 3)

$$\alpha = \begin{cases} 1, & \omega < 0 \\ 1 - \omega/h, & 0 \leq \omega \leq h \\ 0, & \omega > h \end{cases} \quad (3)$$

Here, h denotes the height of the rib. α illustrates the effect of rib height: a higher rib would result in a larger contact area with the same open interface.

In Eq. (2), u_p is the plastic component of relative normal displacement, calculated as

$$u_p = \begin{cases} u_{max} - u_{lim}, & u_{max} \geq u_{lim} \\ 0, & u_{max} < u_{lim} \end{cases} \quad (4)$$

where u_{max} is the maximum normal displacement in the loading history and u_{lim} is the elastic limit of relative normal displacement. Thus, the local compression yielding strength, f_y , in front of the inclined rib is calculated as

$$f_y = E_b u_{lim} \quad (5)$$

All the relative normal displacement defines compression as positive; it is assumed that no contact stress will occur on the tension side.

2.2 Reinforcing bar strain effect on normal contact

The direction of normal contact stress is almost parallel to the Goto cracks (Fig. 2), the width of which denotes the damaged state of the surrounding concrete and can be represented by the bar strain (Shima *et al.* 1987). The concrete compression performance parallel to the crack will decrease as the of transverse crack increases (Collins and Vecchio 1982). Therefore, the increase of bar

strain, i.e. the increase of Goto crack width, will certainly reduce the normal contact stress, which stands for the compressive behavior of such a cracked concrete strut in front of a rib.

Thus, the normal contact stress at an arbitrary location is expressed as follows

$$\sigma_n = \frac{\sigma_n^0}{1 + \varepsilon \times 10^\lambda} \quad (6)$$

where ε is the axis tensile strain of the corresponding rebar element and parameter λ is a constant value to be determined by fitting the model with experiment results.

2.3 Modeling of friction between inclined rib and concrete

According to Eq. (1), an increase of local opening would result in a reduction of u_n and an increase of v_n . Such non-normality of the contact state between ribs and concrete could induce anisotropic damage, especially under insufficient confinement. As a matter of fact, a local wedge effect has been reportedly found in front of the rib (Xu *et al.* 1994). Thus, it is of great necessity to take local friction into account.

The friction along the inclined rib τ_n (compression side) is formulated as follows

$$\begin{cases} d\tau_n = \alpha G_n dv_n \\ \int_{path} d\tau_n \leq \mu \sigma_n \end{cases} \quad (7)$$

where G_n is the tangential stiffness along the inclined rib and is computed as

$$G_n = 0.5E_n \quad (8)$$

The Poisson effect of the interface is denied.

Total friction is assumed to follow the Mohor-Coulomb criterion; the chemical cohesion between steel and concrete is not considered here, and μ is the friction coefficient. According to the experimental results by Xu *et al.* (1994), μ is around 0.2~0.3 (in this paper, $\mu = 0.25$).

2.4 Spatial average model of bond for three-dimensional analysis

For 3D FE analysis, the spatial average bond stress and dilatant stress in the finite domain can be computed as follows

$$\begin{cases} \tau_b = \frac{1}{L}(\sigma_n \sin \theta + \tau_n \cos \theta) \\ \tau_\varphi = E_\varphi \delta_\varphi \\ \sigma = \frac{1}{L}(-\sigma_n \cos \theta + \tau_n \sin \theta) \end{cases} \quad (9)$$

L denotes the spacing of ribs in a longitudinal direction; τ_φ , E_φ and δ_φ are the shear stress, stiffness and shear slip along the hoop direction of the rebar (Fig. 4). Considering that the torsion of the reinforcing bar seldom occurs in the structure, it is reasonable to assume elastic behavior in the hoop direction of the bar with relatively large stiffness.

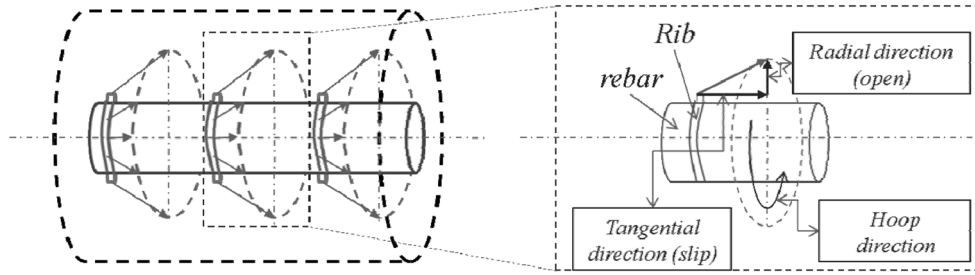


Fig. 4 Three-dimensional strain field of interface for bond

3. Parameter study

3.1 General discussion

In the formulations (1)-(9), θ , h and L are the geometric characteristics of the reinforcing bars, which are controlled by the manufacturing code for reinforcing bar in each country. In this study, these parameters follow the codes of China and Japan, according to each experiment. Therefore, only parameters E_n , f_y and λ need to be studied.

Sensitivity analyses were carried out to simulate Shima *et al.*'s (1987) experiments (case of 10D

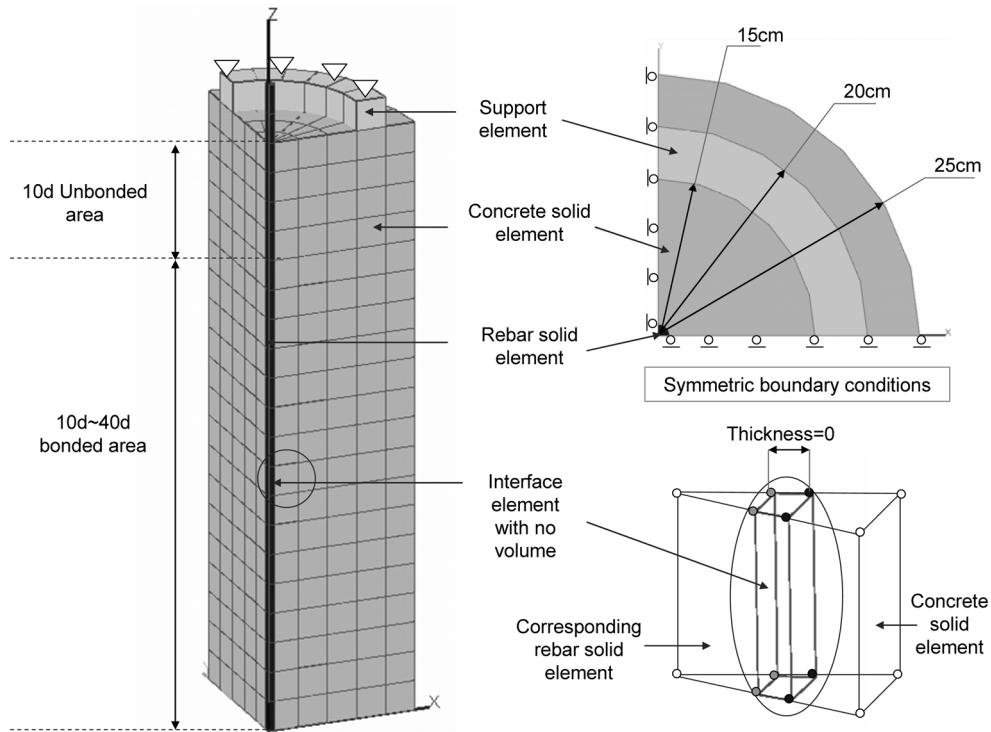


Fig. 5 Mesh discretization for simulation of Shima *et al.*'s experiment

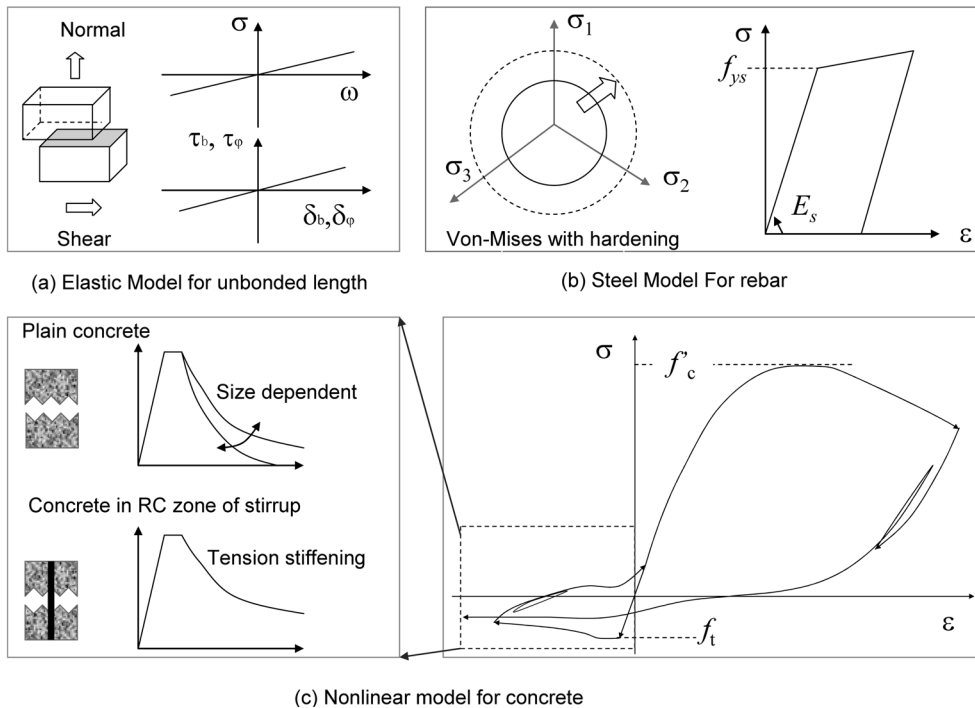


Fig. 6 Numerical models for rebar, concrete and unbonded areas

embedment length) for our parameter study. The 3D FE mesh discretization is shown in Fig. 5 as well as the setting of boundary conditions. A 1/4 symmetric model was used for analysis as the splitting crack was avoided in this case. The open-slip coupled bond model was applied to the bonded area. To simulate the 10D-unbonded length in the experiment, interface elements were used with elastic models and extremely small stiffness in both open and shear directions as shown in Fig. 6(a).

As discussed, 3D-quadrilateral solid elements were applied to both the reinforcing bar and the surrounding concrete. The rebar is simulated by the elasto-plastic Von Mises model with hardening as shown in Fig. 6(b).

For the solid concrete element prior to cracking, a 3D elasto-plastic and continuum fracture model was used (Maekawa and Okamura 1983, Hauke and Maekawa 1999). After cracking, the fixed multi-directional smeared crack approach was used (Fukuura and Maekawa 1998). Thus, the interaction between Goto cracks and splitting cracks were simulated. And the constitutive laws for tension, compression and shear transfer (Okamura and Maekawa 1991) were employed to describes the nonlinear behavior of cracked concrete (Fig. 5(c)). The concrete elements were regarded as plain concrete, according to the zoning procedures (An *et al.* 1997). The residual tension stress strain relationship was adjusted according to the mesh size (Fig. 5(c)), depending on the fracture energy of the concrete (Bazant and Oh 1983). All of these models have been well verified in past research (Maekawa *et al.* 2003), and so the details are omitted here. In Table 1, concrete strength is 30 MPa and bar properties are as shown.

Table 1 Bar properties used in Shima *et al.*'s experiment

Diameter (mm)	Young's modulus (GPa)		Yielding strength (MPa)		θ	h (mm)	L (mm)
	Steel	Aluminum	Steel	Aluminum			
19.5	190	72	366	450	45°	1.5	9.9

3.2 Study of E_n and f_y

As discussed, the bond mechanism is similar to the cracking shear transfer problems. As a matter of fact, the bond is governed by rib-aggregate interaction, while cracking shear is transferred by aggregate-aggregate interaction. As the elastic modulus and strength of the steel are much larger than that of the aggregate, the deformation and local yielding will be mainly located on the side of aggregate rather than the rib. Therefore, the formulation of contact stiffness E_b and local yielding strength f_y can refer to the research on the cracking shear transfer (Maekawa *et al.* 2003), which is expressed as follows

$$\begin{cases} E_b = 343f_c'^{(1/3)} & (\text{MPa/mm}) \\ f_y = 13.7f_c'^{(1/3)} & (\text{MPa/mm}) \end{cases} \quad (10)$$

3.3 Study of λ

As discussed in section 2.2, parameter λ is set to quantify the effect of bar strain on bond. Finite

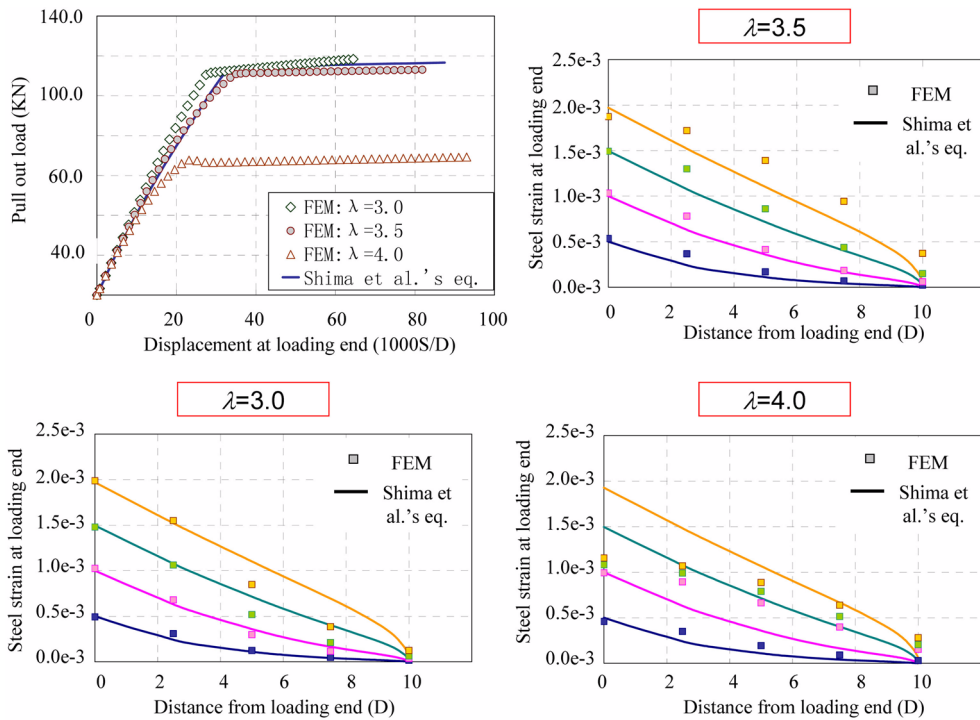


Fig. 7 Simulation of Shima *et al.*'s experiment (10D embedment) with large mesh

analyses with settings of $\lambda = 3.0$, $\lambda = 3.5$ and $\lambda = 4.0$ were carried out; the load-slip data (at the loading end) and steel strain distribution along the longitudinal direction were selected from the FE analysis results for comparison with the results computed by Shima *et al.*'s equation (1987), as shown in Fig. 7. Obviously for the best accuracy we have

$$\lambda = 3.5 \tag{11}$$

3.4 Mesh sensitivity

FE analysis with much finer mesh was carried out, and the parameters were set as Eqs. (10) and (11). Fig. 8 shows the analytical results of steel strain distribution along the reinforcing bar. The parameters of E_b , f_y and λ were found to be applicable to different sizes of mesh.

3.5 Sensitivity of concrete strength

The sensitivity of the concrete's strength was checked by FE analysis of Shima *et al.*'s experiment (10D embedment) with different concrete strengths, then compared with Shima *et al.*'s equation, as shown in Fig. 9. The effect of concrete strength on bonds can be roughlyly captured with the Eqs. (10) and (11).

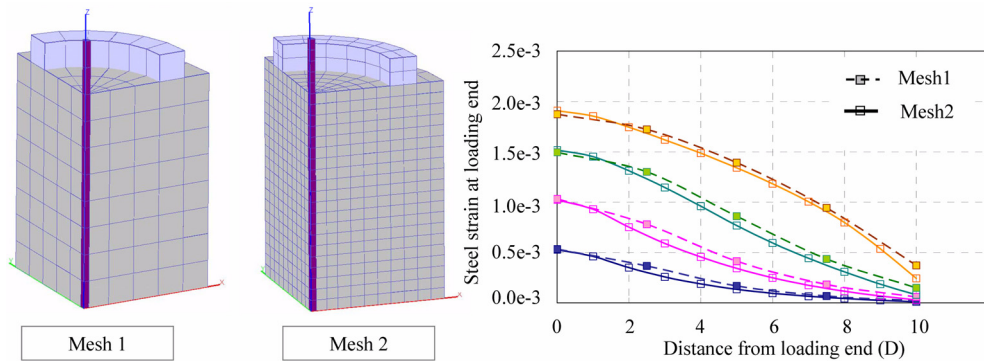


Fig. 8 Mesh sensitivity of simulation of Shima *et al.*'s experiment (10D embedment) with $\lambda = 3.5$

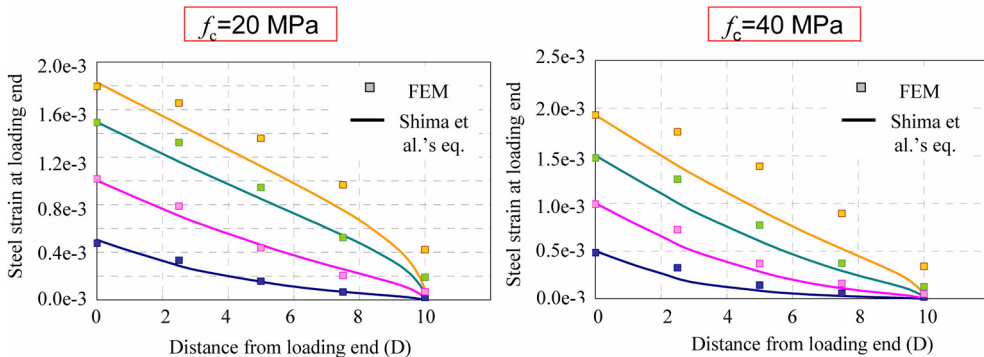


Fig. 9 Simulation of Shima *et al.*'s experiment (10D embedment) with different concrete strengths

The local bond performance could be significantly influenced by local bleeding of concrete due to casting method and mix portions. The porous conditions beside the reinforcing bar would be even worse than that between the aggregate and hardened cement paste (Salem and Maekawa 2003). Therefore, it is hardly possible to have a universal formulation for concrete strength that includes all the effects above. Eqs. (10) and (11) can be accepted for the same reasons as Shima *et al.*'s experiment: normal concrete with a casting direction opposite to the pull-out direction. Strictly speaking, this should be modified with consideration of different casting and mixing details. However, in this paper, it is rational to use these two for the general discussion of bond mechanisms.

4. Verification

4.1 Simulation of pull-out experiments with extremely long embedded bar

Bond performance is affected by the embedded length of rebar, and bond strength varies for different location along reinforcing bar. However, extremely long embeddings of reinforcing bar, which leads to zero strain and zero slip at the free end in pull-out experiments, result in independency of bar location for the local slip and steel strain. And the steel strain distribution at any loading step can be simply obtained as a parallel translation of a uniquely shaped curve

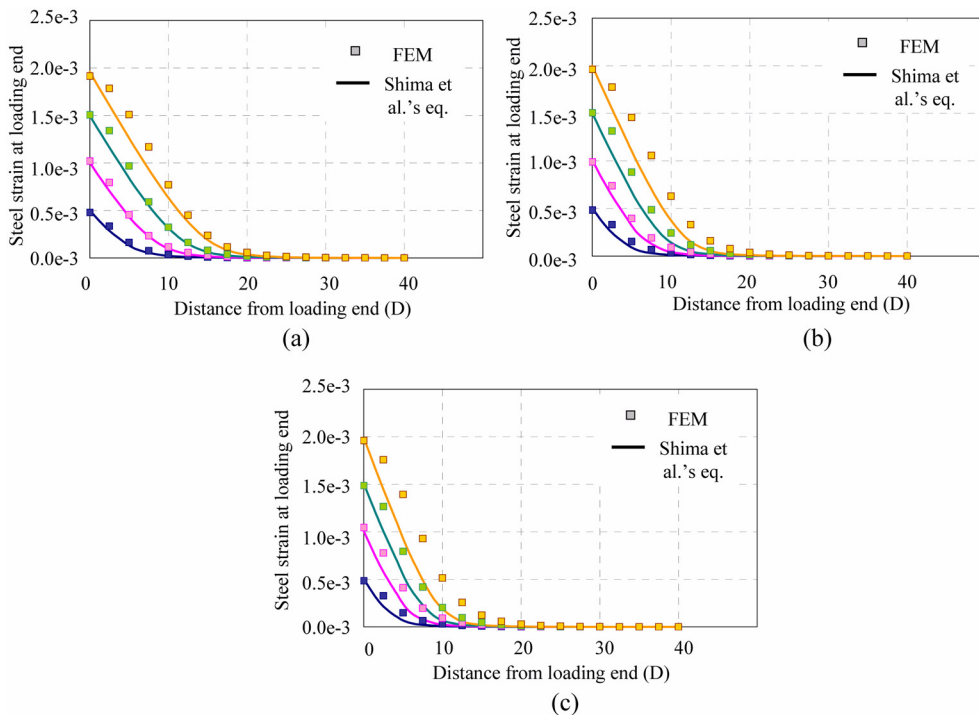


Fig. 10 Simulation of Shima *et al.*'s experiment (40D embedment) with different concrete strengths; (a) Steel bar; 40D embedment; $f_c = 20$ MPa, (b) Steel bar; 40D embedment; $f_c = 30$ MPa, (c) Steel bar; 40D embedment; $f_c = 40$ MPa

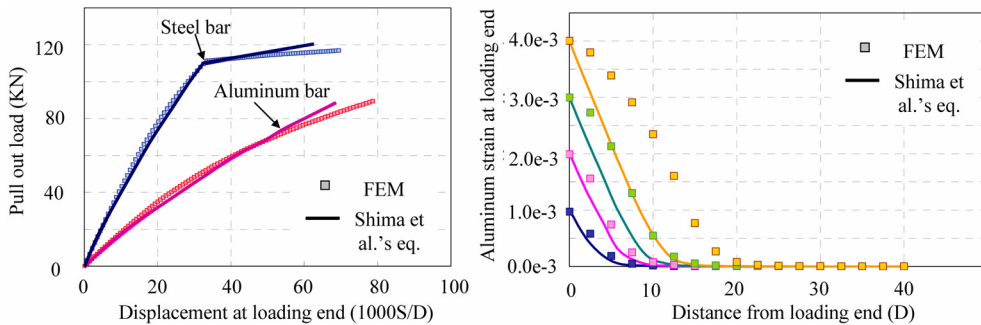


Fig. 11 Simulation of Shima *et al.*'s experiments (40D embedment) with aluminum bar

(Maekawa *et al.* 2003). The 40D embedment pull-out experiments by Shima *et al.* (1987) were simulated with the open-slip coupled modeling as discussed. A similar FE mesh discretization as in Fig. 5 was used. The effect of concrete strength was also checked. Figs. 10(a)~(c) shows the FE analytical results compared with Shima *et al.*'s equation, with good agreement.

4.2 Simulation of pull-out experiments with aluminum bar

Shima *et al.* (1987) also conducted a pull-out experiment with aluminum bar that had the same geometry as for steel rebar (Table 1). It was found that the bond stress of aluminum rebar is much smaller than that of steel bar, which illustrates well the rebar strain effects on bonds.

FE analysis successfully simulated this experiment. Close agreement was found for the load-slip relationship (at the loading end) and some overestimation of aluminum strain penetration from the loading end tends to occur when the aluminum bar strain at loading end is larger than 3,000 micros, which implied an underestimation of local bond performance (Fig. 11). However, for conventional reinforced concrete with steel bars, it is rational to have such an underestimation as the post-yielding response for safety.

4.3 Simulation of pull-out experiments with insufficient concrete cover

Unlike Shima *et al.*'s case, conventional reinforced concrete structures have a larger risk of bond failure due to splitting of the concrete cover. Thus, it is of great importance to study the propagation of splitting cracks induced by steel-concrete bonds. The pull-out experiment conducted by Xu *et al.* (1994) was simulated to verify the applicability of the open-slip coupled model.

Fig. 12(a) shows the FE mesh discretization. The same treatment as Shima *et al.*'s case was applied to concrete/steel solid elements and bonded/unbonded interfaces between reinforcing bar and concrete. To simulate the splitting behavior, a complete model was used. Table 2 shows the characteristics of rebar used for simulation of Xu *et al.*'s experiment, according to the manufacturing code of China.

Table 2 Bar properties used for simulation of Xu *et al.*'s experiment

Diameter (mm)	Young's modulus (GPa)	Yielding strength (MPa)	θ	h (mm)	L (mm)
16	181	337.5	45°	0.1	1.0

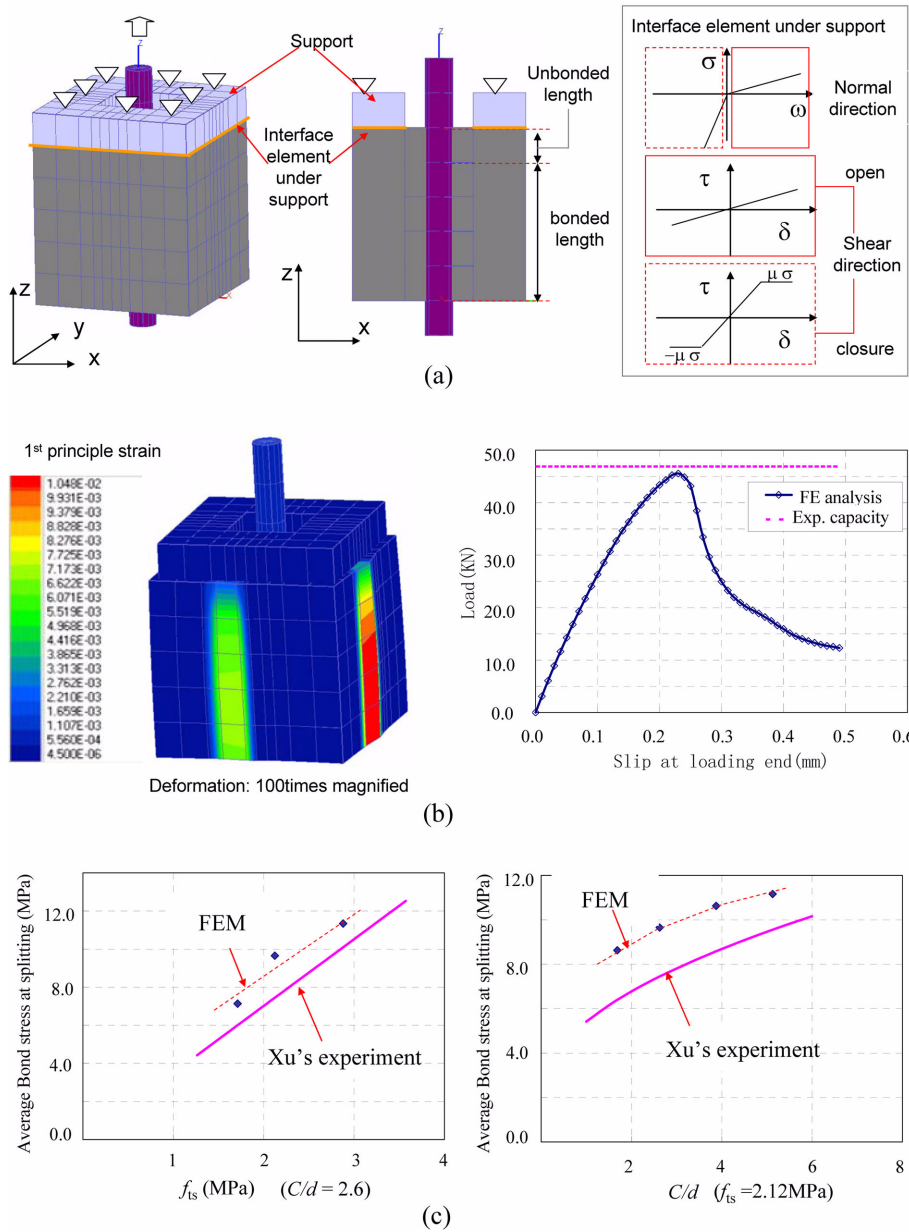


Fig. 12 (a) Mesh detail for FE simulation of Xu *et al.*'s experiments, (b) FE simulation of Xu *et al.*'s experiments with splitting failure ($f_c = 30$ MPa, $C = 42$ mm, $\rho_{sv} = 0\%$) and (c) Simulation of Xu *et al.*'s experiments with the sensitivity of f_{ts} and C/d

To simulate the complex contact conditions between the support and the specimen, another interface element had to be used. A bi-linear stress strain relationship was applied to this interface element, which assumes very small stiffness for both normal and shear directions when the interface has a positive open and large stiffness in the negative case. Mohor-Coulomb friction was also assumed in

the shear direction for the closure case (Fig. 12(a)). Fig. 12(b) shows a load-slip relationship (at the loading end) by FE analysis of Xu *et al.*'s experiment and the experimental capacity can be well captured. Numerical splitting crack can also be obtained as shown in the first principle strain contour image.

FE analyses were also carried out to study the sensitivity of concrete strength and C/d on the splitting effect. Fig. 12(c) shows the simulation results. Here, f_{ts} means the splitting tensile strength of concrete. The tendency of Xu *et al.*'s experiment can be well captured, whereas FE analyses overestimated a little, due to the fact that the concrete strength of most of Xu *et al.*'s specimens were within 30 MPa and the casting direction was perpendicular to the reinforcement. Serious bleeding could occur and lead to a weak porous zone around the reinforcement and significantly reduce the bond performance (Salem & Maekawa 2003).

5. Strain effect and splitting effect on open-slip of interface

Fig. 13 shows the local opening and local slip of the interface along the reinforcing bar in 10D and 40D embedment cases by FE analyses. In both cases, local opening is two orders less than local slip at the interface due to the large confinement by the huge concrete cover. Besides, for short bar embedded cases, a negative local opening can be found at the free end, i.e., the steel-concrete interface tends to be closed, which leads to a much higher local bond strength than that at other location.

Fig. 14 shows the local opening and local slip of the interface along the aluminum bar. Compared with steel bar's case, the local slip of the interface along the aluminum bar is much larger, but local

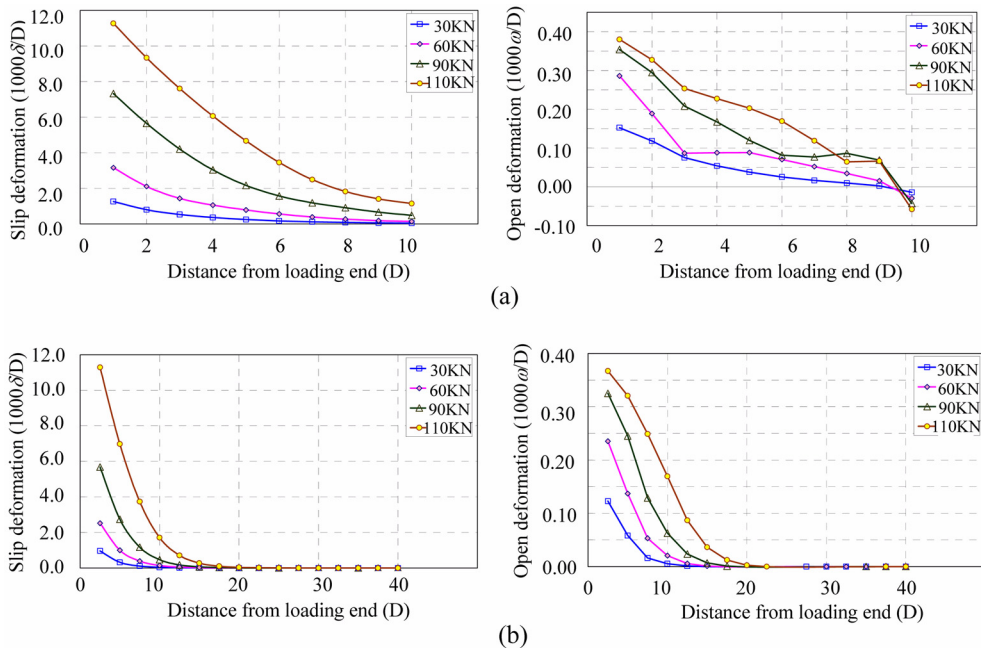


Fig. 13 FE analytical open-local slip of Shima *et al.*'s experiments along bars; (a) Steel bar; 10D embedment; $f_c = 30$ MPa, (b) Steel bar; 40D embedment; $f_c = 30$ MPa

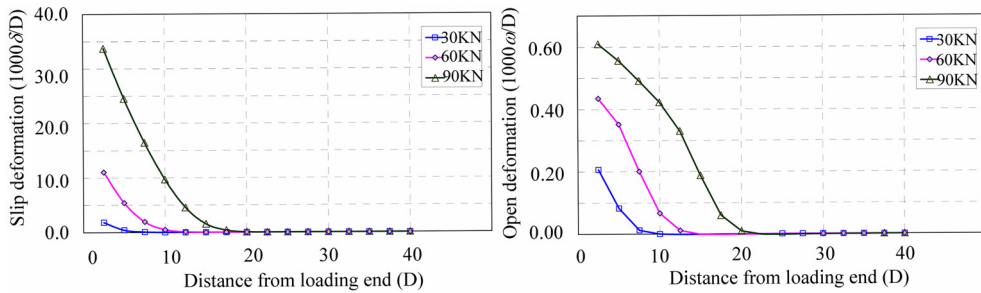


Fig. 14 FE analytical open-slip of Shima *et al.*'s experiments along aluminum bars

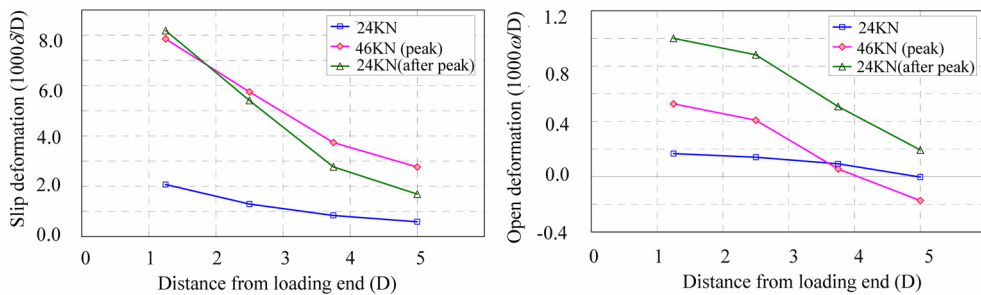


Fig. 15 Open-local slip of Xu *et al.*'s experiments ($f_c = 30$ MPa, $C = 42$ mm, $\rho_{sv} = 0\%$)

opening does not change much. This means Shima *et al.*'s (1987) case stands for the loading path with a large local slip but a small local opening on the interface.

Fig. 15 shows the local opening and local slip of the interface along the reinforcing bar from Xu *et al.*'s experiment. The rapid increase of local opening occurs when the splitting crack penetrates the concrete cover, while local slip does not change much after its peak state. This suggests that Xu *et al.*'s case and Shima *et al.*'s case represent two extremely different states of bonds, both of which can be successfully simulated by an open-slip model.

Great similarity can be found in the cracking shear transfer problems. The loading path with a small open of cracking does not lead to deterioration of the shear transfer (Li and Maekawa 1989), while a large opening is the source of shear softening along the cracks (Bujadham *et al.* 1990, 1992, Mishima *et al.* 1992). Thus, the open-slip deformation of the interface should be incorporated to evaluate the bonding characteristics of reinforcing bar.

6. Sensitivity of bar geometry: extended to plain rebar's case

Rebar's surface geometry is known to significantly affect its bonding performance. Generally speaking, the bond strength of deformed rebar is much larger than for plain rebar due to the existence of a rib, the height of which is about 1 mm. However, the physical image of general surface roughness concentration for the case of plain bar is quite similar to that for a rib, which might have different h , θ and L . Therefore, it is possible to extend the above model to plain bar's case.

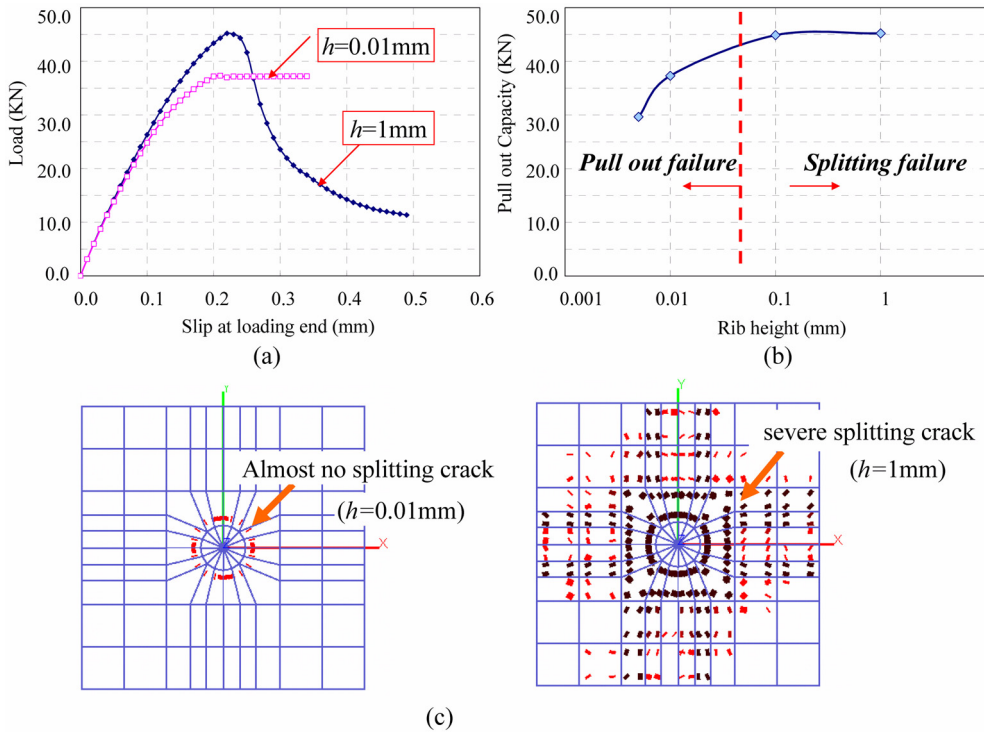


Fig. 16 Sensitivity analysis results of different h ; (a) Typical load-displacement relationship, (b) Effect of rib height on pull out capacity, (c) Typical rack image at top surface of specimen for different failure pattern

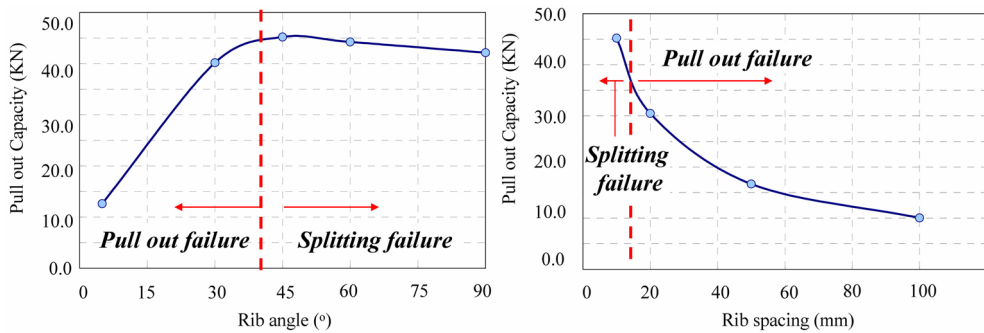


Fig. 17 Sensitivity analysis results of different θ (left figure) and L (right figure)

A series of sensitivity analyses were carried out to study the effect of bar geometry. The case of Xu *et al.*'s pull-out specimen ($h = 1\text{ mm}$, $\theta = 45^{\circ}$ and $L = 10\text{ mm}$) was used as the standard case. The effects of h , θ and L were also studied.

Figs. 16(a)-(c) show the typical analytical result of different h . The pull-out capacity would be reduced as h decreases. Furthermore, the analytical failure pattern could change from splitting failure to pull-out failure when h becomes smaller, which coincides with the general experimental facts: deformed reinforcing bar leads to splitting failure, while plain bar results in pull-out failure.

According to Xu *et al.*'s (1994) measurements, the maximum height of roughness concentration for plain bar is about 0.025~0.04 mm, while the analysis also indicates that the case of $h = 0.01$ mm shows almost no splitting crack. Thus, the open-slip model could be reasonably accurate for a general discussion of bar geometry.

Similar results can be obtained in the sensitivity analyses of θ and L . Fig. 17 shows the results, that smaller θ and larger L could lead to pull-out failure, while the opposite cases end with splitting failure. Also, a too large rib angle could cause a reduction of pull-out capacity as the splitting crack appears much faster than the smaller one.

7. Conclusions

An open-slip coupled bond model was developed for the three-dimensional FE analysis of reinforced concrete. Both strain and splitting effects were simulated with this model. The analysis proves that the strain effect results from a large local slip, while the splitting effect is from the large open-slip.

As a matter of fact, the open-slip of the interface represents the local deformation of the concrete that is close to the reinforcing bar. Slip represents the longitudinal deformation along the reinforcing bar that is dominated by Goto crack width, and opening represents the radial deformation that is governed by splitting crack width. This implies that such local concrete deformation has a great influence on bond. This is due to large difference in the stiffness and strength between rebar and concrete, which locates all the damage in the concrete. Thus, both local opening and local slip have to be considered in bond modeling. This can be further extended to the case after the reinforcing bars corrode.

The sensitivity of bar geometry can also be studied with this model. It demonstrates the significance of bar geometry on the failure pattern and proves that the open-slip coupled model can be applied to plain bar's case.

References

- An, X., Shawky, A.A. and Maekawa, K. (1997), "The collapse mechanism of a subway station during the Great Hanshin earthquake", *Cement Concrete Compos.*, **19**, 241-257.
- Ayoub, A. and Filippou, F.C. (1999), "Mixed formulation of bond-slip problems under cyclic loads", *J. Struct. Eng.*, **125**(6), 661-671.
- Bazant, Z.P. and Oh, B.J. (1983), "Crack band theory for fracture of concrete", *Mater. Struct.*, **16**, 155-157.
- Bujadham, B. and Maekawa, K. (1992), "The universal model for stress transfer across cracks in concrete", *Proceedings of JSCE*, **17**(451), 277-287.
- Bujadham, B., Maekawa, K. and Mishima, T. (1990), "Cyclic discrete crack modeling for reinforced concrete", *Computer Aided Analysis and Design of Reinforced Concrete Structures*, Pineridge Press, 1225-1236.
- Cox, J.V. and Herrmann, L.R. (1998), "Development of a plasticity bond model for steel reinforcement", *Mech. Cohes.-Frict. Mater.*, **3**, 155-180.
- Collins, M.P. and Vecchio, F. (1989), "The response of reinforced concrete to in-plane shear and normal stresses", *University of Toronto*, 1982.
- Chou, L., Niwa, J. and Okamura, H. (1983), "Bond model for deformed bars embedded in massive concrete", *Proc. of 2nd JCI Colloquium on Shear Analysis of RC Structures*, JCI. 42-52.
- Fukuura, N. and Maekawa, K. (1998), "Multi-directional crack model for in-plane reinforced concrete under

- reversed cyclic actions-Four-way fixed crack formulation and verification”, *Comput. Model. Concrete Struct., Euro-C*, 143-152.
- Gambarova, P., Rosati, G. and Zasso, B. (1989), “Steel-to-concrete bond after concrete splitting: constitutive laws and interface deterioration”, *Mater. Struct.*, **22**, 347-356.
- Goto, Y. (1971), “Cracks formed in concrete around deformed tension bars”, *ACI J. Proceedings*, **68**(4), 244-251.
- Hawkins, N.M., Lin I.J. and Jeang, F.L. (1982), “Local bond strength of concrete for cyclic reversed loading”, *Bond in concrete*, Applied Science Publishers, London, 151-161.
- Hauke, B. and Maekawa, K. (1999), “Three-dimensional modeling of reinforced concrete with multi-directional cracking”, *J. Mater. Concrete Struct. Pavements*, JSCE, **45**(634), 349-368.
- Jendele, L and Cervenka J. (2006), “Finite element modeling of reinforcement with bond”, *Comp. Struct.*, **84**, 1780-1791.
- Li, B., Maekawa, K. and Okamura, H. (1989), “Contact density model for stress transfer across crack in concrete”, *J. Fac. Eng. Univ. Tokyo (B)*, **40**(1), 9-52.
- Lura, P., Plizzari, G.A. and Riva, P. (2002), “3D finite-element modelling of splitting crack propagation”, *Mag. Concrete Res.*, **54**(6), 481-493.
- Maekawa, K. and Okamura, H. (1983), “The deformational behavior and constitutive equation of concrete using the elasto-plastic and fracture model”, *J. Fac. Eng., Univ. Tokyo (B)*, **37**(2), 253-328.
- Maekawa, K., Pimanmas, A. and Okamura, H. (2003), “*Nonlinear mechanics of reinforced concrete*”, Spon Press, London.
- Mishima, T., Yamada, K. and Maekawa, K. (1992), “Localized deformational behavior of a crack in RC plates subjected to reversed cyclic loads”, *Proceedings of JSCE*, **16**(442), 161-170.
- Okamura, H. and Maekawa, K. (1991), “*Nonlinear analysis and constitutive models of reinforced concrete*”, Gihodo Press, Tokyo.
- Ragueneau, F., Dominguez, N. and Ibrahimbegovic, A. (2006), “Thermodynamic-based interface model for cohesive brittle materials: application to bond slip in RC structures”, *Comput. Method. Appl. M.*, **195**, 7249-7263.
- Shima, H., Chou, L. and Okamura, H. (1987), “Micro and macro models for bond in reinforced concrete”, *J. Fac. Eng., Univ. Tokyo (B)*, **39**(2), 133-194.
- Salem, H.S. and Maekawa, K. (2003), “Pre- and postyield finite element method simulation of bond of ribbed reinforcing bars”, *J. Struct. Eng.*, **130**(4), 671-680.
- Tassios, T.P. and Yannopoulos, P.J. (1981), “Analytical studies on reinforced concrete members under cyclic loading based on bond stress-slip relations”, *ACI J.*, **5**(6), 206-216.
- Teng, Z. and Zou, L. (1996), “Nonlinear Finite element analysis of RC members under reversed cyclic loading”, *China Civil Eng. J.*, **43**(2), 17-29. (in Chinese)
- Xu, Y.L., Shen, W.D. and Wang, H. (1994), “An experimental study of bond-anchorage properties of bars in concrete”, *J. Build. Struct.*, **15**(3), 27-36. (in Chinese)